Optics and Lasers in Engineering 137 (2020) 106382

Contents lists available at ScienceDirect

Optics and Lasers in Engineering

journal homepage: www.elsevier.com/locate/optlaseng

High-resolution real-time 360° 3D surface defect inspection with fringe projection profilometry

Jiaming Qian[a,b], Shijie Feng[a,b], Mingzhu Xu[a,b], Tianyang Tao[a,b], Yuhao Shang[a,b], Qian Chen[a], Chao Zuo[a,b,*]

[a] Smart Computational Imaging (SCI) Laboratory, Nanjing University of Science and Technology, Nanjing, Jiangsu Province 210094, China
[b] Jiangsu Key Laboratory of Spectral Imaging & Intelligent Sense, Nanjing University of Science and Technology, Nanjing, Jiangsu Province 210094, China

ARTICLE INFO

Keywords:
Fringe projection profilometry (FPP)
3D Imaging
Point cloud registration
Surface defect inspection

ABSTRACT

Since a slight variance in production processes can make the entire production run defective, defect inspections are indispensable procedures in manufacturing processes to ensure high quality of each item before entering the next manufacturing step. Three-dimensional (3D) optical shape measurement technologies are widely applied for surface defect inspection of complex workpieces because of its high-accuracy and digitization. However, the complex surface structure and position of the test object can pose serious challenges, making inspections still relatively slow, expensive, and complicated in implementation and maintenance. In this work, we propose a real-time 360° 3D surface defect inspection approach based on fringe projection profilometry without any auxiliary equipment for position control. Firstly, a multi-view 3D measurement based on geometric constraints is employed to acquire high-accuracy depth information from different perspectives. Then, a cycle-positioning-based registration scheme with the establishment of the pose-information-matched 3D standard digital model is proposed to realize rapid alignment of the measured point cloud and the standard model. Finally, a minimum 3D distance search is driven by a dual-thread processing mechanism for simultaneous scanning and detecting to quantify and locate 3D surface defects in real time. Experimental results show that our method can accurately identify the surface defects of complicated objects in real time in an extremely simple (hand-held) manner, saving a lot of operational expenses on precision alignment and position-orientation adjustment. The proposed method holds tremendous potential for quality control in many facets of industry, such as product development, testing, and manufacturing.

1. Introduction

With the advent of industry 4.0, the emerging from the Industrial Internet of Things and data science prompts the traditional manufacturing industry to accelerate towards intelligence [1,2]. In the field of intelligent manufacturing, how to ensure high quality standards at a competitive cost through rapid and accurate industrial inspection is one of the biggest challenges [3]. Optical quality control, which usually contains two-dimensional (2D) and three-dimensional (3D) inspection methods, plays an important role in modern defect inspection technologies because of its more reliable inspection accuracy, higher inspection efficiency and more automated inspection means than traditional manual inspection methods [4]. Compared with 2D visual inspection [5–7], 3D defect detection technologies are preferred for surface quality control owing to its insensitivity to factors such as shadow, angle, and illumination [4].

The 3D surface defect inspection technology is to (1) firstly employ the 3D visual measurement to extract the 3D point cloud data of the surface of the object, (2) then register the acquired point cloud and the discretized standard CAD model or the 3D model of the defect-free object, and (3) finally calculate the deviation between them [8]. (1) 3D reconstruction is the basis of the entire inspection process, whose quality is directly related to the inspection accuracy. Fringe projection profilometry (FPP) [9–11] is one of the most popular non-contact 3D optical measurement techniques because of its advantages of high measurement accuracy, simple hardware facilities and flexible implementation, which has been widely applied to obtain high-quality 3D surface information of complex objects [12–14]. (2) The registration between the measured point cloud and the discretized standard model is the biggest challenge in 3D defect inspection. Due to the uncertainty of the relative pose between the 3D point clouds to be registered, it is difficult to rapidly achieve 3D matching with a general registration

* Corresponding author at: Nanjing University of Science and Technology, Nanjing University of Science and Technology Xiao Ling Wei Street #200 Nanjing, Jiangsu 210094, China.
E-mail addresses: ShijieFeng@njust.edu.cn (S. Feng), chenqian@njust.edu.cn (Q. Chen), zuochao@njust.edu.cn (C. Zuo).

https://doi.org/10.1016/j.optlaseng.2020.106382
Received 1 July 2020; Received in revised form 9 September 2020; Accepted 14 September 2020
0143-8166/© 2020 Published by Elsevier Ltd.

algorithm. Researchers usually align measurement data and standard data from two directions [8,15,16]. The first direction obtains the transformation matrices used for coarse registration in advance through strict restrictions on the relative position of the object and the imaging system (which often depends on some special clamps and robotic arms or rotary stages)[8,15,17]. Such instrument-assisted methods fundamentally avoid the diversity of the initial posture of the measured point cloud by controlling the position of the object with special clamps and presetting the scanning path of the imaging system with robotic arms or rotary stages, but it requires high hardware cost and complicated time-consuming preprocessing. Besides, the clamps need to be specially customized for different objects, and their use hinders the scanning and inspection of the clamping regions of the object. In the second direction, some professional point cloud processing tools [18] are applied to manually select several 3D matching points of the two point clouds to be matched or move them to roughly aligned positions to carry out registration [16,19,20]. Compared with the first scheme, this method is more economical, but the transfer of data and human intervention greatly reduce the matching efficiency, making it even more time-consuming than traditional manual inspection. (3) In addition, in order to realize the detection of views of the object from all sides, the current 3D surface defect inspection scheme usually adopts the way of first measuring the object from different perspectives and fusing the measured point cloud data, and then performing error detection [8,15], which on the one hand introduces cumulative registering errors into the measurement data, on the other hand, makes the entire inspection process more time-consuming. A more efficient way is to realize real-time defect inspection. In industrial manufacturing,"real-time inspection" to a greater extent means "on-line inspection", that is, through the equipment directly installed on the production line, the workpiece can be scanned and inspected simultaneously, so as to provide quick feedback to better guide the production.

From the above discussion, it is not difficult to find that although 3D surface defect inspection is essential for intelligent manufacturing, existing methods have many disadvantages, such as the inability to balance efficiency and cost, the need for additional hardware support and the time-consuming strategy of scanning first and then detecting. Ideally, the object should be scanned and detected simultaneously in real time with as little human intervention as possible without any additional expensive positioning auxiliary. In this work, we propose a high-resolution real-time 3D surface defect inspection technology based on FPP for complicated workpieces without any auxiliary equipment for position and orientation control. We utilize the stereo phase unwrapping (SPU) technique assisted by adaptive depth constraint (ADC) strategy to achieve high-accuracy real-time 3D data acquisition from a single perspective. Then, a fast posture-information-matched 3D standard digital model establishment approach based on simultaneous localization and mapping (SLAM) technology is proposed to deal with the diversity of initial attitudes of measured point cloud. Next, to rapidly align the measurement data with the standard model, a cycle-positioning-based registration algorithm is developed. Besides, we propose a simple minimum 3D distance retrieval method for 3D surface defect calculation. Finally, a dual-thread parallel mechanism for simultaneous alignment and detection is constructed to further improve the inspection efficiency. In order to verify the validity of our approach, a quad-camera real-time 3D imaging device and a software integrating 3D data acquisition, point cloud data registration, standard library establishment and 3D defect calculation are developed. The experimental results show that our method can perform simultaneous real-time 3D scanning and 3D defect inspection on complicated objects without any additional positioning equipment assistance and expensive pre/post-processing, which is more economical, convenient and efficient than traditional methods. Specifically, compared with the current state-of-the-art method (robot-arm-assisted method), our method has three main advantages. Firstly, we can realize automatic 3D point cloud registration without auxiliary position control devices such as robotic arms and clamps, so the hardware cost is greatly reduced, and the entire system is simpler. Secondly, our approach can perform real-time simultaneous scanning and inspection. Different from the conventional method of scanning and registering and then performing the post-processing of inspection, our approach is significantly more efficient and can provide industrial assembly line feedback in time to adjust production. Thirdly, the conventional method of first registering all 3D measurement information of the test object may bring about accumulated registration errors. In our method of scanning while detecting, the registration of each measurement data and the standard model is carried out independently, thus avoiding the introduction of accumulated registration errors in the measurement data.

2. Principle

2.1. Real time 3D information acquisition from a single perspective

Whether for real-time 3D model reconstruction or real-time surface defect inspection, rapid 3D data acquisition is necessary. At present, the 3D imaging technologies based on structured light illumination have developed into one of the most widely applied 3D measurement methods, which can be divided into surface structured illumination technology and line structured light illumination technology. In terms of speed, the single full-field imaging of the surface structured light method is significantly superior to the measurement mode of the line-scanning-based handheld 3D scanners [21–23]. Regarding accuracy, the accuracy of 3D products based on line structured light will decrease in the actual measurement due to the continuous stitching of measurement data to complete surface scanning. Therefore, in this work, we employ a 3D imaging technology based on surface structured illumination—fringe projection profilometry (FPP). The two mainstream phase analysis techniques of FPP are phase-shifting (PS) methods [24,25] and Fourier-transform (FT) methods [26–29]. The former has high measurement resolution, high measurement accuracy and robustness to environmental interference due to the contribution of multi-step (usually at least three-step) PS images in the time domain. However, multi-frame time-domain information will reduce the imaging efficiency and increase the sensitivity to motion, so the PS methods will be corrupted when measuring dynamic objects, especially when the motion between frames is non-negligible. In recent years, with the development of high-speed projection and imaging devices, high-speed high-accuracy 3D measurement based on PS has gradually become possible [30–33]. The latter is well-known for its single-shot attribute, and can extract phase signals through frequency domain analysis. However, spectrum aliasing caused by sharp edges, discontinuous, and/or large surface reflectivity variation areas makes it difficult to separate effective phase information, which limits the imaging quality of FT in these areas. Since accuracy is crucial during defect inspection, we choose PS methods in this work. Considering the efficiency issue, meanwhile, the three-step PS method is finally adopted. The three-step PS fringe patterns are projected by the projector onto the object, and then captured by the camera after being modulated by the object. The captured images can be expressed as:

$$I_n(x,y) = A(x,y) + B(x,y)\cos(\phi(x,y) + 2\pi n/N), \tag{1}$$

where (x, y) represents the image pixel coordinate, I_n is the captured $(n+1)$th fringe image, $n \in [0, 2]$, A denotes the average intensity, B is the amplitude, ϕ is the phase, and $2\pi n/N$ is the phase shift. With PS algorithm, the phase ϕ can be acquired:

$$\phi(x,y) = -\arctan\frac{\sqrt{3}\left(I_1^c(x,y) - I_2^c(x,y)\right)}{2I_0^c(x,y) - I_1^c(x,y) - I_2^c(x,y)}. \tag{2}$$

Due to the truncation feature of the *arctan* function, only the wrapped phase (ranging from $-\pi/2$ to $\pi/2$) can be obtained. The signs of the numerator and denominator of Eq. (2) can be further used to uniquely define a quadrant for each calculation of ϕ, and the phase values at

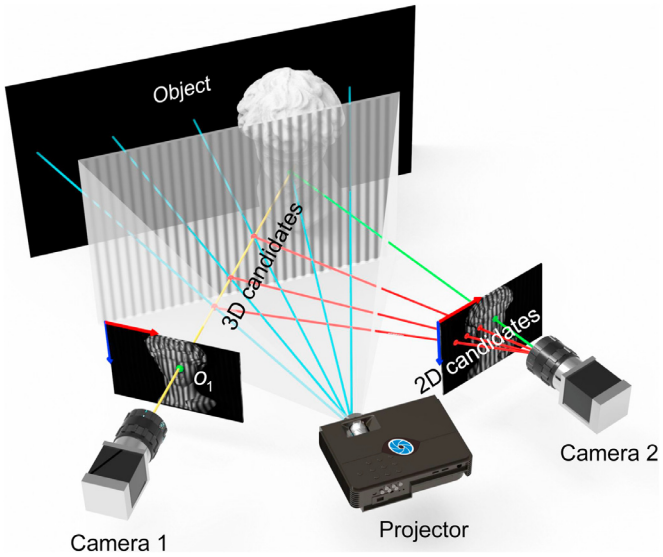

Fig. 1. The principle of SPU.

each point can be determined from $-\pi$ to π with the 4-quadrant arctangent. To recover the absolute phase, the common practice is to use the temporal phase unwrapping (TPU) methods [34,35], which determine the pixel-wise fringe order with the unique wrapped phase distribution in the time domain. However, TPU usually needs to project additional Gray-code patterns or multi-wavelength fringes, which greatly decreases the efficiency of phase unwrapping. Recently, the stereo phase unwrapping (SPU) method [36–38] based on geometric constraint can solve the phase ambiguity problem without any additional auxiliary images. Although more cameras (at least two) are required than traditional FPP system, SPU does maximize the efficiency of phase unwrapping and is well-suitable to real-time 3D measurement in dynamic scenarios. A typical SPU-based FPP system consists of a projector and two cameras, the principle of which can be seen in Fig. 1. If the number of used fringes is K, for an arbitrary point o_1 on Camera 1, there are K possible fringe orders $(0, 1, 2, \dots, K-1)$, which corresponds to K possible absolute phases. With these possible absolute phases, K possible 3D candidate points can be reconstructed by the calibration parameters [39–41] between Camera 1 and the projector, as shown by the intersections of the yellow line emitted by Camera 1 and the blue line emitted by the projector in Fig. 1. The retrieved 3D candidates can be projected to Camera 2 to obtain K 2D candidates by the calibration parameters between Camera 2 and the projector, as shown by the red and green 2D points of Camera 2 in Fig. 1. Among these 2D candidates, there must be a correct matching point (the green 2D candidate of Camera 2 in Fig. 1) which has a more similar wrapped phase value to o_1 than other candidates. According to this feature, the phase consistency check is performed to determine the correct matching point (it is worth mentioning that the 2D candidates of Camera 2 can continue to be projected onto a third or even fourth camera for phase consistency checking to further rule out more incorrect candidates), and then 3D reconstruction can be carried out with the calibration parameters between Camera 1 and Camera 2 [42]. However, factors such as calibration errors and ambient light interference may cause some erroneous 2D candidates to have a more similar phase value to o_1 than the correct matching point. The adaptive depth constraint (ADC) strategy [43], which updates pixel-wise depth constraint range in real time to eliminate most erroneous 3D candidates before the phase consistency check, can effectively improve the stability of SPU. Therefore, through utilizing SPU and assisted by ADC, we can measure high-accuracy 3D data in real time from a single perspective.

2.2. Standard library creation

In order to achieve defect inspection, there must be a standard reference, which is usually a scanned complete 3D model of a standard/defect-free workpiece or an existing standard CAD model. In our approach, we focus on how to obtain the full-scale 3D measurement of a standard workpiece to make the standard library for reference, which is closely related to the efficiency of subsequent 3D surface defect detection.

To rapidly realize the 3D digitization of complete shapes of a standard workpiece, our previous work of high-resolution real-time 360° 3D model reconstruction [44] is utilized. Due to the limitation of the field of view of the imaging system, the object must be rotated relative to the measurement system (or the latter must be moved relative to the former) to acquire and register views of the object from all sides. 3D point cloud registration usually includes coarse registration and fine registration. For coarse registration, traditional methods often require the assistance of additional instruments, such as rotary stages [17] and robotic arms [15]. However, due to expensive hardware structures and time-consuming pre-processing, the instrument-assisted registration methods are not the ideal means to obtain a 360° 3D model. A better solution, which is also a great challenge, is to rotate the target arbitrarily and complete the 3D matching in real time without any additional auxiliary instruments. To this end, we improve the simultaneous localization and mapping (SLAM) technology [45] used for map construction and localization of robots in unknown environment, so as to realize fast rough registration. We define the measured 3D point clouds and the corresponding 2D texture maps at two adjacent moments when the object is rotating as XYZ_1, XYZ_2 and I_1, I_2, respectively. Firstly, the Scale Invariant Feature Transformation (SIFT) algorithm [46] is applied to locate and match the 2D feature points of I_1 and I_2, which can be mapped to the corresponding 3D matching points. According to the characteristics of 3D matching points, which is that distances between a 3D point and others in XYZ_1 should be similar to those in XYZ_2, we can exclude some wrong matching point pairs. With the optimized 2D and 3D matching points and the pre-calibrated camera internal parameters, the transformation matrices between the 3D matching points can be quickly calculated according to the EPnP method [47], which is a non-iterative technology for estimating camera pose from n correspondences between 3D reference points in visual SLAM systems. Then, XYZ_1 can be roughly aligned with XYZ_2 through the obtained rotation and translation matrices. After achieving coarse registration, the iterative closest point (ICP) technology [48] is performed for fine registration. In order to further improve the registration efficiency and reduce the cumulative matching error, a dual-thread parallel mechanism is developed for simultaneous coarse and fine registration. We use the sum of the two norms of the rotation and translation vectors to quantify the relative motion of the object during each coarse registration. Only when the cumulative motion amount reaches a certain threshold, the ICP-based fine registration is performed in a separate thread, during which the coarse registration can be continued in the coarse registration thread.

Through the above methods, we can rapidly scan a standard workpiece and build its complete 3D geometric models $XYZ^{standard}$. Suppose that there are total h effective registering elements in the scanning process, the corresponding 2D texture images of which can be expressed as $I_1 - I_h$. We employ the coarse and fine registration transformation matrices obtained in the modeling process to rotate the acquired 3D model $XYZ^{standard}$ to the original posture of each 2D image and express the transformed models as $XYZ_1^{standard} - XYZ_h^{standard}$ (the reason why we transform $XYZ^{standard}$ will be explained in the next section). Finally, we store $I_1 - I_h$ and the 3D models $XYZ_1^{standard} - XYZ_h^{standard}$ as the standard library for reference, as shown in Fig. 2.

It is worth mentioning that our approach of standard library creation is also applicable to the existing standard CAD model. We can firstly use some professional 3D processing tools such as MeshLab or Geomagic

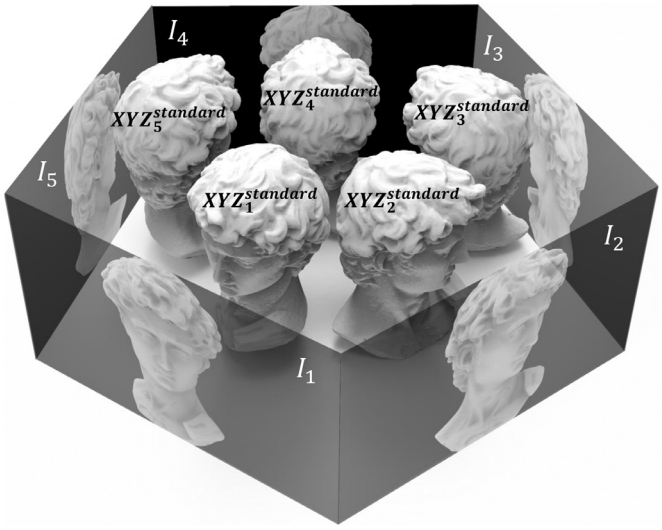

Fig. 2. The created standard library. It contains the 2D texture images $I_1 - I_h$ of total h effective registering elements in the scanning process and the 3D models $XYZ_1^{complete} - XYZ_h^{complete}$ in the original postures of the h 2D images.

studio to align $XYZ^{standard}$ and existing standard CAD model XYZ^{CAD}, then transform XYZ^{CAD} to $XYZ_1^{CAD} - XYZ_h^{CAD}$ corresponding the original postures of $I_1 - I_h$ by using the obtained transformation matrices, and finally store $I_1 - I_h$ and $XYZ_1^{CAD} - XYZ_h^{CAD}$ as the standard library.

2.3. 3D surface defect inspection

After establishing the standard 3D model, we can scan the measured workpiece and perform surface defect inspection. The traditional 3D inspection scheme is usually to first obtain all the 3D shapes of the measured object and stitch them into a complete 3D model, then artificially register the measured point cloud and the standard model in the 3D processing tool (otherwise expensive hardware facilities and complex preprocessing are needed), and finally analyze the differences between them to obtain the surface defects of the measured object [8,15,16]. However, the manual intervention makes the inspection process inconvenient in practice, while the auxiliary mechanical devices make the whole system expensive and difficult to implement. In addition, the operation of scanning and fusing first and then registering and detecting not only introduces the effect of accumulated registration errors, but also makes the entire inspection process more time-consuming. Ideally, the object should be scanned and detected at the same time with as little human intervention as possible without additional auxiliary equipment. The biggest challenge to achieve this is how to automatically align the scanned 3D point cloud with the standard 3D model. Due to the poor relative initial posture between the measured data and the standard model, rapidly registering them through algorithm is difficult, which is also why the traditional methods require manual intervention or mechanical assistance. In the previous section, we have explained how to adopt SLAM to achieve fast coarse matching of the point cloud slices in two adjacent perspectives, but the registration must rely on 2D texture images with sufficient matching pairs. In order to construct such a relationship between the measured point cloud XYZ_c of the current perspective and the 3D standard model $XYZ^{standard}$, we employ the 2D images $I_1 - I_h$ in the standard library to rapidly locate the pose that has the most overlap with XYZ_c, and then realize the alignment of XYZ_c and $XYZ^{standard}$, followed by defect inspection. In addition, to further improve the efficiency of the whole detection process, we separately put registration and inspection in two parallel threads for synchronization. The flowchart of the proposed 3D surface defect inspection approach is shown in Fig. 3. Next, we will first introduce the principle of registration between the measured data and the standard model, then discuss our proposed inspection approach in detail, and finally explain the dual-thread structure for simultaneous registration and detection.

Step 1: we utilize the Oriented Fast and Rotated Brief (ORB) technology [49], whose efficiency is two orders of magnitude higher than SIFT, to sequentially find the 2D matching points between the 2D texture map I_c of the measured object under current pose and $I_1 - I_h$ in the standard library. Then, the 2D image I_i ($i \in [1, h]$) in the standard database having the most matching points with I_c is determined, which overlaps the current measurement view the most and can ensure reliable subsequent alignment. **Step 2:** we again use SIFT to more accurately locate the 2D matching points of I_i and I_c. **Step 3:** with the found 2D matching pairs, their corresponding 3D points in XYZ_c and the pre-calibrated camera internal parameters, the transformation matrices from the posture of XYZ_c to I_i's can be solved by EPnP. However, the posture of $XYZ^{standard}$ is not consistent with that of I_i, signifying that XYZ_c cannot be aligned with $XYZ^{standard}$ even if it is transformed. Fortunately, we have rotated $XYZ^{standard}$ to the original pose of I_i in advance, so the calculated transformation matrices can be used directly to roughly register XYZ_c with $XYZ_i^{standard}$. **Step 4:** ICP is carried out to achieve fine registration of XYZ_c and $XYZ_i^{standard}$, the iteration of which can converge to the correct registration result faster in case of good relative pose estimated by coarse registration.

Then we will discuss the difference comparison between XYZ_c and $XYZ_i^{standard}$. As shown in Fig. 4, for an arbitrary 3D point O in XYZ_c, its matching point in $XYZ_i^{standard}$ is O'. Compared with other points $O'_1 - O'_4$ near O', O' has the closest distance to point O. Based on such feature of 3D matching points, we utilize the smallest distance between O and all 3D points of $XYZ_i^{standard}$ to judge the 3D surface defect of O. However, if the distances between the 3D points in $XYZ_i^{standard}$ are greater than those in XYZ_c, errors may be introduced to such a defect calculation strategy. Fortunately, $XYZ_i^{standard}$ is composed of multiple point cloud slices with overlapping parts, so its density is much greater than XYZ_c, which guarantees the accuracy of this defect calculation approach. Another issue to consider is that the 3D defect at point O (the distance between O and O') may be greater than the distance between O and $O'_1 - O'_4$, which leads to defect misjudgment. However, defects are generally in a block rather than a few points, so the above phenomenon will only occur at several points on the edge of the defect region, which has little impact on the positioning of the whole defect region. Eventually, the 3D surface defects of the measured object at the current view can be located and quantified by such a minimum distance retrieval operation for every 3D points of XYZ_c pixel by pixel in GPU (**Step 5**).

In order to further improve the inspection efficiency, we propose another dual-thread parallel mechanism for simultaneous alignment and detection. After the registration of XYZ_c and $XYZ_i^{standard}$ in the alignment thread, the 3D surface defects are calculated in the inspection thread while the measured object can continue to be rotated to complete the registration between the measured point cloud data of another perspective and the standard 3D model. Since the proposed inspection strategy is to detect while scanning, it not only greatly improves the detection efficiency, but also avoids the accumulated stitching errors (because each registration is done separately instead of continuing to accumulate registration based on the last registration). After each inspection, the detected point clouds can be directly spliced together according to the relationship between the measured point cloud and the standard model (the measured point cloud has been aligned with the standard model and each standard model can be converted to each other by the transformation matrices obtained during the database building process). The entire detection algorithm flow is as follows:

Step 1: Utilize ORB to find I_i in the standard database having the most matching points with I_c;

Step 2: More accurately locate the 2D matching points of I_i and I_c by using SIFT;

Step 3: Calculate the transformation matrices from the posture of XYZ_c to I_i's with EPnP and roughly register XYZ_c and $XYZ_i^{standard}$;

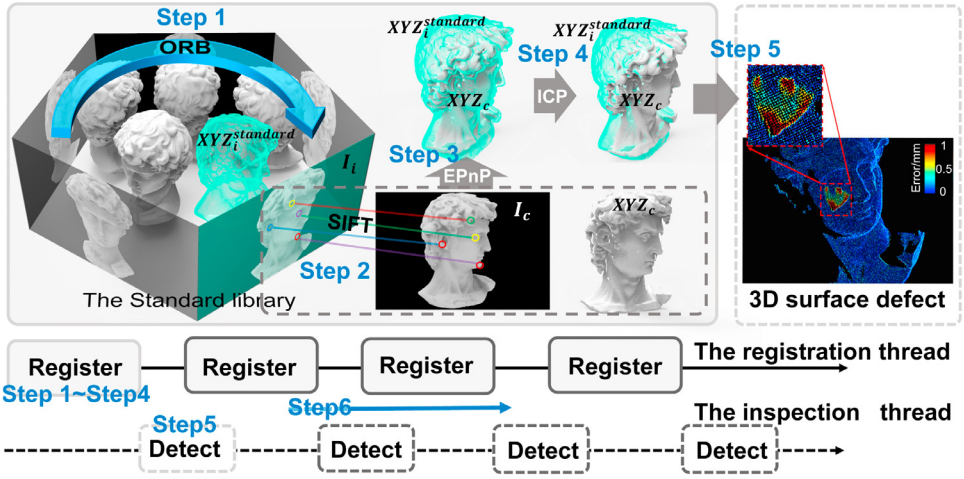

Fig. 3. The flowchart of the 3D surface defect inspection approach. **Step 1:** Utilize ORB to find I_i in the standard library having the most matching points with I_c; **Step 2:** Locate more accurate 2D matching points of I_i and I_c by SIFT; **Step 3:** Roughly register XYZ_c and $XYZ_i^{standard}$ with EPnP; **Step 4:** Perform ICP to realize fine registration; **Step 5:** Obtain the 3D surface defect of XYZ_c by minimum distance retrieval operation for every 3D points of XYZ_c in GPU and in a separate defect inspection thread; **Step 6:** Rotate the measured object to the next perspective and repeat the above steps to obtain its 3D surface defect until all 360° surfaces of the measured object are detected.

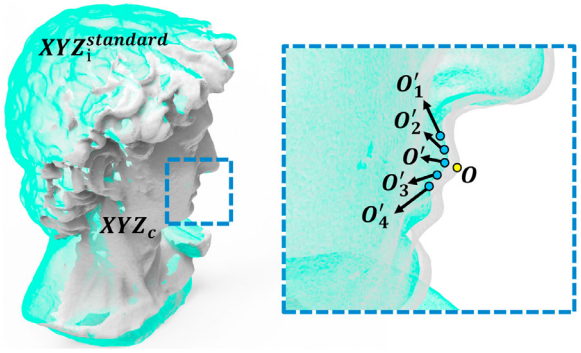

Fig. 4. The principle of defect calculation: the smallest distance between O and all 3D points of $XYZ_i^{standard}$ is used to judge the 3D surface defect of O. Note that XYZ_c and $XYZ_i^{standard}$ will be well-merged in practice, and the large gap in the illustration is intended to better explain the detection principle.

Step 4: Perform ICP to realize fine registration;

Step 5: Locate and quantify the 3D surface defect of XYZ_c by minimum distance retrieval operation for every 3D points of XYZ_c in GPU and in a separate defect detection thread;

Step 6: Rotate the measured object to the next perspective and repeat the above steps to obtain its 3D surface defect until all 360° surfaces of the measured object are detected.

3. Experiments

In order to verify the validity of our approach, we construct a SPU-based FPP system, which contains 4 Basler acA640-750 cameras (640 × 480 resolution) and a LightCraf ter 4500 (912 × 1140 resolution). All cameras are triggered synchronously by the projector. The speed of the projector is 100Hz, and 48-period 3-step PS fringe patterns are used. We use a HP Z230 computer (Intel Xeon E3-1226 v3 CPU, NVIDIA Quadro K2200 GPU) to develop our algorithm based on Qt, OpenCV, PCL and CUDA. The imaging speed of the system is 45 Hz, the single scanning accuracy is 45 μm and the overall 360° registering accuracy is up to 100 μm level [44].

Firstly, a David plaster model is measured. We rotate the David model arbitrarily in front of the built 3D scanner by hand and synthesize its 3D surface shapes from multiple single perspectives in real time as the standard 3D model $XYZ^{standard}$. Through the transformation matrices obtained during the merging process, $XYZ^{standard}$ is quickly rotated to the original poses of the 2D images $I_1 - I_{12}$ in effective registration perspectives. The transformed 3D models $XYZ_1^{standard} - XYZ_{12}^{standard}$ and the corresponding 2D images $I_1 - I_{12}$ are made into as the standard library. Fig. 5 shows some of the library files, and the whole scanning and database building process can be seen in Visualization 1. We paste some paper on David's nose to simulate defects. Then the defective David model is arbitrarily rotated and scanned, and its 3D surface defects are detected in real time. The inspection scene at a certain moment is shown in Fig. 6, and the whole inspection process can be seen in Visualization 2. The time for single registration and detection is about 2.08 s and 1.31 s, respectively. Fig. 7 shows the final defect inspection results of the defective David model, where Fig. 7(a)-(c) are the David model with 'pasted' defect from different perspectives, and Fig. 7(d)-(f) are the detected 3D defect results from different perspectives. We use pseudo color to indicate the size of the defect, and users can visually observe the size and location of the defect according to the color change (the range of which can be adjusted). In this work, the deviation we calculate and display is actually the absolute value of the deviation, and its sign can be directly represented by the positive and negative signs of the depth difference between the standard model and the measured data. It can be seen from the inspection results that the regions with defects are well determined, as shown in red dotted frames in Fig. 7, while the others do not show any flaw as they should. It should be noted that, as mentioned above, defects often appear in a block rather than a few scattered points, so the individual discrete points with large defect values which are caused by noise in the scanning process do not represent defects.

Finally, we inspect a outer end cover of generator with the proposed approach. We first model a standard workpiece and generate the standard library for reference. Then a measured workpiece is detected by our approach. In order to verify the accuracy of our detecting approach, we also apply the professional 3D processing tool MeshLab to detect the measured workpiece. The defect inspection results by using our method and MeshLab are shown in Fig. 8, where Fig. 8 (a)-(c) are the standard workpiece from different perspectives, Fig. 8 (d)-(f) are the measured workpiece from different perspectives, Fig. 8 (g)-(i) are the inspection results by MeshLab and Fig. 8 (j)-(l) are the inspection results by our approach. Comparing Figs. 8 (a)-(c) and Figs. 8 (d)-(f), we can find that the defects of the measured workpiece are difficult to be judged by naked eyes or 2D images, which can only be detected by 3D means. In addition, the red mark on the measured workpiece as shown in white dotted frames in Fig. 8 may cause 2D detection methods to misjudge. It can be seen from the comparison between Figs. 8 (g)-(i) and Fig. 8 (j)-(l) that through our approach, the 3D surface defects of the workpiece can be accurately determined, which are very close to the results of professional 3D tool. Due to the need to manually select the 3D matching points between the measured point cloud and the standard model, using MeshLab is often more time-consuming and usually takes a few minutes.

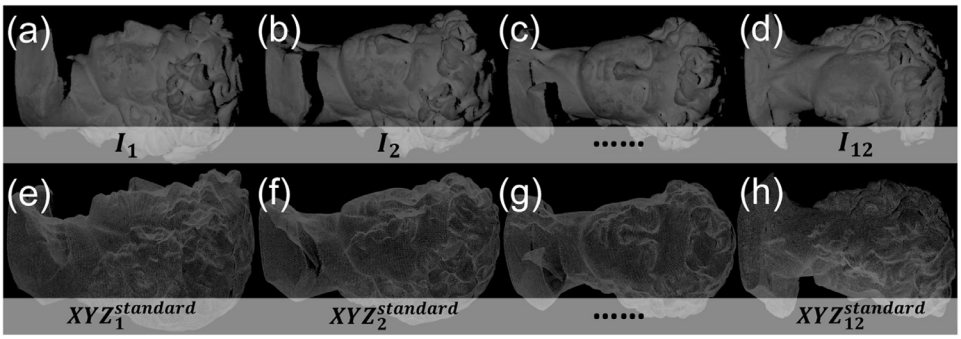

Fig. 5. The standard library of the David model (see Visualization 1 for whole scanning and database building process).

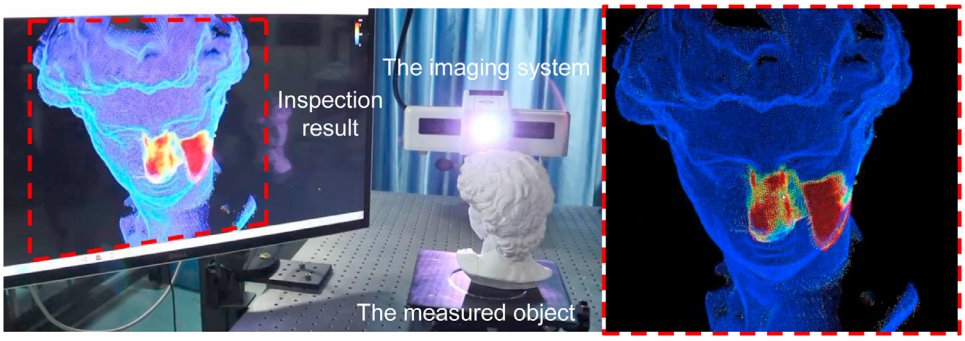

Fig. 6. The detection scene and result at a certain moment (see Visualization 2 for whole detection process).

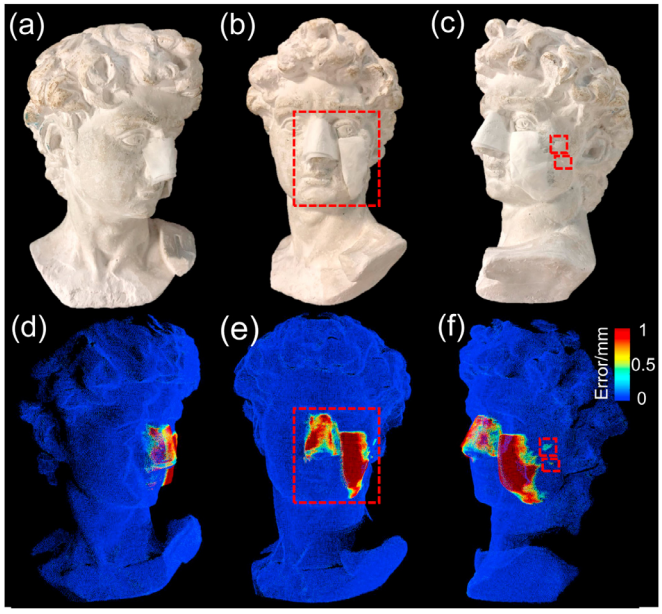

Fig. 7. The final defect inspection results of the David model. (a)-(c) The David model of 'pasted' defect from different perspectives. (d)-(f) The measured 3D surface defect results from different perspectives. We use pseudo color to indicate the size of the defect, and users can visually observe the size and location of the defect according to the color change.

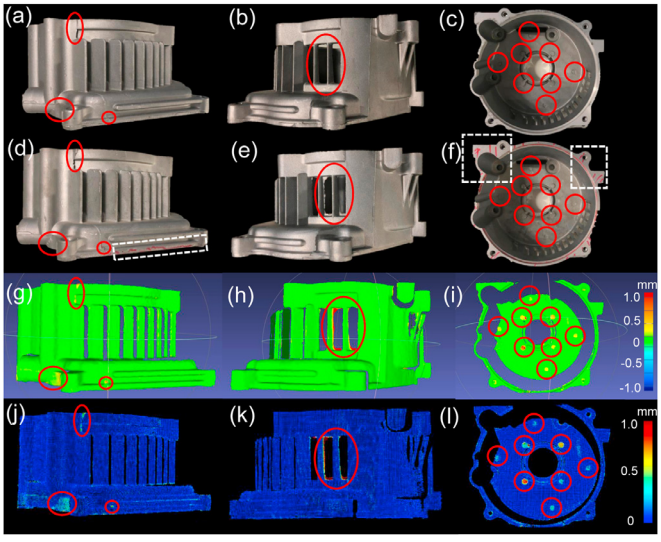

Fig. 8. The defect detection results of a outer end cover of generator. (a)-(c) The standard workpiece from different perspectives. (d)-(f) The measured workpiece from different perspectives. (g)-(i) The detection results by MeshLab. (j)-(l) The detection results by our approach.

Compared with the software detection method, our approach can more efficiently, conveniently and automatically detect the 3D surface defects of the measured object in real time.

4. Conclusion

In this work, we propose a high-resolution real-time 360° 3D surface defect inspection technology, which requires no assistance of any mechanical auxiliary devices. In addition, we develop a software system including real-time high-accuracy 3D data acquisition, real-time point cloud registration and real-time defect inspection functions to verify the feasibility of the proposed algorithm. This work makes low-cost, high-speed, high-quality and easy-to-implement surface defect inspection of complex workpieces possible. We think our technique has the potential to carry out real-time efficient full inspection of workpieces on the factory assembly line with relatively economical equipments, the inspection results of which can be fed back to the production line to adjust the production process in time.

However, there are still several aspects that need to be further improved in the proposed algorithm. The main concern is the memory problem. When detecting larger workpieces, the memory occupied by the standard models with multiple poses will increase sharply, which poses challenges to computer performance. In the future, we will research the data compression technology of 3D point cloud to overcome such difficulty. The second shortcoming is that when reconstructing the 3D model of the standard workpiece, it is inevitable to introduce cumulative stitching errors. Therefore, we recommend using the existing standard CAD models to prepare the standard library that matches attitude information for rapid registration.

We declare that we have no financial and personal relationships with other people or organizations that can inappropriately influence our work, there is no professional or other personal interest of any nature or kind in any product, service and/or company that could be construed as influencing the position presented in, or the review of, the manuscript entitled.

Declaration of Competing Interest

None.

Acknowlgedgments

This work was supported by National Natural Science Foundation of China (61722506, 61705105, 11574152), National Key R&D Program of China (2017YFF0106403), Outstanding Youth Foundation of Jiangsu Province (BK20 170034), Fundamental Research Funds for the Central Universities (30917011204, 30919011222), and Leading Technology of Jiangsu Basic Research Plan (BK20192003).

Supplementary material

Supplementary material associated with this article can be found, in the online version, at 10.1016/j.optlaseng.2020.106382.

References

[1] Ustundag A, Cevikcan E. Industry 4.0: managing the digital transformation. Springer; 2017.
[2] Li L. China'S manufacturing locus in 2025: with a comparison of made-in-china 2025 and industry 4.0. Technol Forecast Soc Change 2018;135:66–74.
[3] Villalbadiez J, Schmidt D, Gevers R, Ordieresmere J, Buchwitz M, Wellbrock W. Deep learning for industrial computer vision quality control in the printing industry 4.0. Sensors 2019;19(18):3987.
[4] Liu S, Wang Q, Luo Y. A review of applications of visual inspection technology based on image processing in the railway industry. Transp Saf Environ 2019;1(3):185–204.
[5] Li Q, Ren S. A visual detection system for rail surface defects. IEEE Trans Syst Man Cybernet Part C (Applications and Reviews) 2012;42(6):1531–42.
[6] Tornero J, Armesto L, Mora MC, Montes N, Herraez A, Asensio J. Defect detection system for car bodies based on artificial vision: desing and implantation. REVISTA IBEROAMERICANA DE AUTOMATICA E INFORMATICA INDUSTRIAL 2012;9(1):93–104.
[7] Fu S, Jiang Z. Research on image-based detection and recognition technologies for cracks on rail surface. In: 2019 International Conference on Robots & Intelligent System (ICRIS). IEEE; 2019. p. 98–101.
[8] Xiong Z, Li Q, Mao Q, Zou Q. A 3d laser profiling system for rail surface defect detection. Sensors 2017;17(8):1791.
[9] Feng S, Zuo C, Tao T, Hu Y, Zhang M, Chen Q, et al. Robust dynamic 3-d measurements with motion-compensated phase-shifting profilometry. Opt Lasers Eng 2018;103:127–38.
[10] Gorthi SS, Rastogi P. Fringe projection techniques: whither we are? Opt Lasers Eng 2010;48(IMAC-REVIEW-2009-001):133–40.
[11] Salvi J, Fernandez S, Pribanic T, Llado X. A state of the art in structured light patterns for surface profilometry. Pattern Recognit 2010;43(8):2666–80.
[12] Zuo C, Chen Q, Gu G, Feng S, Feng F. High-speed three-dimensional profilometry for multiple objects with complex shapes. Opt Express 2012;20(17):19493–510.
[13] Zhang Z. Review of single-shot 3d shape measurement by phase calculation-based fringe projection techniques. Opt Lasers Eng 2012;50(8):1097–106.
[14] Feng S, Zhang L, Zuo C, Tao T, Chen Q, Gu G. High dynamic range 3d measurements with fringe projection profilometry: a review. Meas Sci Technol 2018;29(12):122001.
[15] Han L, Cheng X, Li Z, Zhong K, Shi Y, Jiang H. A robot-driven 3d shape measurement system for automatic quality inspection of thermal objects on a forging production line. Sensors 2018;18(12):4368.
[16] Gabara G, Sawicki P. A new approach for inspection of selected geometric parameters of a railway track using image-based point clouds. Sensors 2018;18(3):791.
[17] Liu X, Peng X, Chen H, He D, Gao BZ. Strategy for automatic and complete three-dimensional optical digitization. Opt Lett 2012;37(15):3126–8.
[18] Niederheiser R, Mokros M, Lange J, Petschko H, Prasicek G, Elberink SO. Deriving 3d point clouds from terrestrial photographs comparison of different sensors and software. In: 23rd congress of the international society of photogrammetry and remote sensing: from human history to the future with spatial information; 2016. p. 685–92.
[19] Han L, Li Z, Zhong K, Cheng X, Luo H, Liu G, et al. Vibration detection and motion compensation for multi-frequency phase-shifting-based 3d sensors. Sensors 2019;19(6):1368.
[20] Zhou P, Zhu J, You Z. 3-D face registration solution with speckle encoding based spatial-temporal logical correlation algorithm. Opt Express 2019;27(15):21004–19.
[21] LI W, ZHAO W, MA P. Reverse technology reseach based on handyscan 3d laser scanner. Mach Tool Hydraulics 2018(7):16.
[22] Redlarski G, Krawczuk M, Pałkowski A. Application of 3d whole body scanning in research on human body surface area; 2017.
[23] Daanen HA, Ter Haar FB. 3D whole body scanners revisited. Displays 2013;34(4):270–5.
[24] Srinivasan V, Liu H-C, Halioua M. Automated phase-measuring profilometry of 3-d diffuse objects. Appl Opt 1984;23(18):3105–8.
[25] Zuo C, Feng S, Huang L, Tao T, Yin W, Chen Q. Phase shifting algorithms for fringe projection profilometry: a review. Opt Lasers Eng 2018;109:23–59.
[26] Takeda M, Ina H, Kobayashi S. Fourier-transform method of fringe-pattern analysis for computer-based topography and interferometry. JosA 1982;72(1):156–60.
[27] Su X, Zhang Q. Dynamic 3-d shape measurement method: a review. Opt Lasers Eng 2010;48(2):191–204.
[28] Kemao Q. Two-dimensional windowed fourier transform for fringe pattern analysis: principles, applications and implementations. Opt Lasers Eng 2007;45(2):304–17.
[29] Huang L, Kemao Q, Pan B, Asundi AK. Comparison of fourier transform, windowed fourier transform, and wavelet transform methods for phase extraction from a single fringe pattern in fringe projection profilometry. Opt Lasers Eng 2010;48(2):141–8.
[30] Zuo C, Chen Q, Gu G, Feng S, Feng F, Li R, et al. High-speed three-dimensional shape measurement for dynamic scenes using bi-frequency tripolar pulse-width-modulation fringe projection. Opt Lasers Eng 2013;51(8):953–60.
[31] Zhang S. Recent progresses on real-time 3d shape measurement using digital fringe projection techniques. Opt Lasers Eng 2010;48(2):149–58.
[32] Qian J, Tao T, Feng S, Chen Q, Zuo C. Motion-artifact-free dynamic 3d shape measurement with hybrid fourier-transform phase-shifting profilometry. Opt Express 2019;27(3):2713–31.
[33] Lei S, Zhang S. Flexible 3-d shape measurement using projector defocusing. Opt Lett 2009;34(20):3080–2.
[34] Zhang Z, Towers CE, Towers DP. Time efficient color fringe projection system for 3d shape and color using optimum 3-frequency selection. Opt Express 2006;14(14):6444–55.
[35] Zuo C, Huang L, Zhang M, Chen Q, Asundi A. Temporal phase unwrapping algorithms for fringe projection profilometry: a comparative review. Opt Lasers Eng 2016;85:84–103.
[36] Weise T, Leibe B, Van Gool L. Fast 3d scanning with automatic motion compensation. In: 2007 IEEE Conference on Computer Vision and Pattern Recognition. IEEE; 2007. p. 1–8.
[37] Tao T, Chen Q, Da J, Feng S, Hu Y, Zuo C. Real-time 3-d shape measurement with composite phase-shifting fringes and multi-view system. Opt Express 2016;24(18):20253–69.
[38] Lohry W, Zhang S. High-speed absolute three-dimensional shape measurement using three binary dithered patterns. Opt Express 2014;22(22):26752–62.
[39] Zhang S, Huang PS. Novel method for structured light system calibration. Opt Eng 2006;45(8):083601.
[40] Yin Y, Peng X, Li A, Liu X, Gao BZ. Calibration of fringe projection profilometry with bundle adjustment strategy. Opt Lett 2012;37(4):542–4.
[41] Huang L, Zhang Q, Asundi A. Camera calibration with active phase target: improvement on feature detection and optimization. Opt Lett 2013;38(9):1446–8.
[42] Liu K. Real-time 3-d reconstruction by means of structured light illumination; 2010.
[43] Tao T, Chen Q, Feng S, Qian J, Hu Y, Huang L, et al. High-speed real–time 3d shape measurement based on adaptive depth constraint. Opt Express 2018;26(17):22440–56.
[44] Qian J, Feng S, Tao T, Hu Y, Liu K, Wu S, et al. High-resolution real-time 360° 3d model reconstruction of a handheld object with fringe projection profilometry. Opt Lett 2019;44(23):5751–4.
[45] Mur-Artal R, Montiel JMM, Tardos JD. Orb-slam: a versatile and accurate monocular slam system. IEEE Trans Rob 2015;31(5):1147–63.
[46] Lowe DG. Distinctive image features from scale-invariant keypoints. Int J Comput Vis 2004;60(2):91–110.
[47] Lepetit V, Moreno-Noguer F, Fua P. Epnp: an accurate o (n) solution to the pnp problem. Int J Comput Vis 2009;81(2):155.
[48] Besl PJ, McKay ND. Method for registration of 3-d shapes. In: Sensor fusion IV: control paradigms and data structures, 1611. International Society for Optics and Photonics; 1992. p. 586–606.
[49] Rublee E, Rabaud V, Konolige K, Bradski G. Orb: An efficient alternative to sift or surf. In: 2011 International conference on computer vision. Ieee; 2011. p. 2564–71.